A Combined Experimental-Numerical Method to Evaluate Powder Thermal Properties in Laser Powder Bed Fusion

Bo Cheng[1]
Industrial Engineering Department,
University of Louisville,
Louisville, KY 40292
e-mail: bcheng1@crimson.ua.edu

Brandon Lane
Engineering Laboratory,
National Institute of Standards and Technology,
Gaithersburg, MD 20899
e-mail: brandon.lane@nist.gov

Justin Whiting
Engineering Laboratory,
National Institute of Standards and Technology,
Gaithersburg, MD 20899
e-mail: justin.whiting@nist.gov

Kevin Chou
Industrial Engineering Department,
University of Louisville,
Louisville, KY 40292
e-mail: kevin.chou@louisville.edu

Powder bed metal additive manufacturing (AM) utilizes a high-energy heat source scanning at the surface of a powder layer in a predefined area to be melted and solidified to fabricate parts layer by layer. It is known that powder bed metal AM is primarily a thermal process, and further, heat conduction is the dominant heat transfer mode in the process. Hence, understanding the powder bed thermal conductivity is crucial to process temperature predictions, because powder thermal conductivity could be substantially different from its solid counterpart. On the other hand, measuring the powder thermal conductivity is a challenging task. The objective of this study is to investigate the powder thermal conductivity using a method that combines a thermal diffusivity measurement technique and a numerical heat transfer model. In the experimental aspect, disk-shaped samples, with powder inside, made by a laser powder bed fusion (LPBF) system, are measured using a laser flash system to obtain the thermal diffusivity and the normalized temperature history during testing. In parallel, a finite element (FE) model is developed to simulate the transient heat transfer of the laser flash process. The numerical model was first validated using reference material testing. Then, the model is extended to incorporate powder enclosed in an LPBF sample with thermal properties to be determined using an inverse method to approximate the simulation results to the thermal data from the experiments. In order to include the powder particles' contribution in the measurement, an improved model geometry, which improves the contact condition between powder particles and the sample solid shell, has been tested. A multipoint optimization inverse heat transfer method is used to calculate the powder thermal conductivity. From this study, the thermal conductivity of a nickel alloy 625 powder in powder bed conditions is estimated to be 1.01 W/m K at 500 °C. [DOI: 10.1115/1.4040877]

Keywords: laser powder bed fusion (LPBF), finite element (FE) model, laser flash, powder bed, thermal conductivity, diffusivity

Introduction

In laser powder bed fusion (LPBF) or powder bed electron beam additive manufacturing (EBAM), the presence of seemingly randomly arranged metallic particles has a significant effect on the process physical phenomenon, e.g., heat transfer. The thermal conductivity of a powder bed in LPBF or EBAM is very different from its solid counterpart due to limited contact between particles in packing conditions. On the other hand, the ability to predict the thermal behavior in metal additive manufacturing (AM) processes is essential to process understanding and part quality improvements. Cheng et al. [1] demonstrated the necessity of including the powder thermal conductivity in modeling heat transfer in EBAM; the measured titanium alloy (Ti-6Al-4V) powder thermal conductivity is less than 15% of the solid Ti-6Al-4V conductivity. In addition, there have been increased modeling studies of powder bed AM processes that consider powder material properties, such as the conductivity and the packing density [2–7]. It has been indicated that the thermal properties of powder materials are critical to the model prediction accuracy.

Information from literature indicates that the specific heat and the latent heat of fusion of metallic powder could be assumed the same as the solid [8–14]. On the other hand, thermal conductivity is more complexly related to powder properties such as porosity or density, therefore has elicited development of several analytical models to estimate conductivity based on these properties. Tolochko et al. [14] developed a mathematical model for the powder thermal conductivity, which considered the effective conductivity due to radiation heat transfer and powder particle contact necks, as well as conduction from gas filling inside the pores in a powder bed. Sih and Barlow [11] presented a porosity-dependent conductivity model for a metallic powder bed. The conductivity of the gas, the porosity, the solid conductivity, and the particle to particle contact-area ratio were taken into account. Moreover, Hadley [15] also developed a model that considered the powder bed porosity and the gas around powder particles. It was reported that predictions made using these equations show reasonable agreement with published metallic powder conductivity.

Measuring powder thermal properties for LPBF is not a trivial task. The powder conditions within the measurement apparatus ought to replicate those within an LPBF system during a build process. A laser flash apparatus, used to measure material thermal diffusivity, may enable closer replication of in situ powder conditions. Laser flash apparatus was developed based on a study by Parker et al. [16]. The authors utilized a light source to heat a disk-shaped sample from one side with a sensor to detect the thermal signal rise on the other side of the sample. Figure 1 shows a general configuration of a laser flash system; a pulse laser energy input is applied to a flat surface of the sample in a very short duration (order of ms) and the temperature response from the opposite

[1]Corresponding author.

Manuscript received June 27, 2018; final manuscript received July 6, 2018; published online August 22, 2018. Editor: Y. Lawrence Yao.

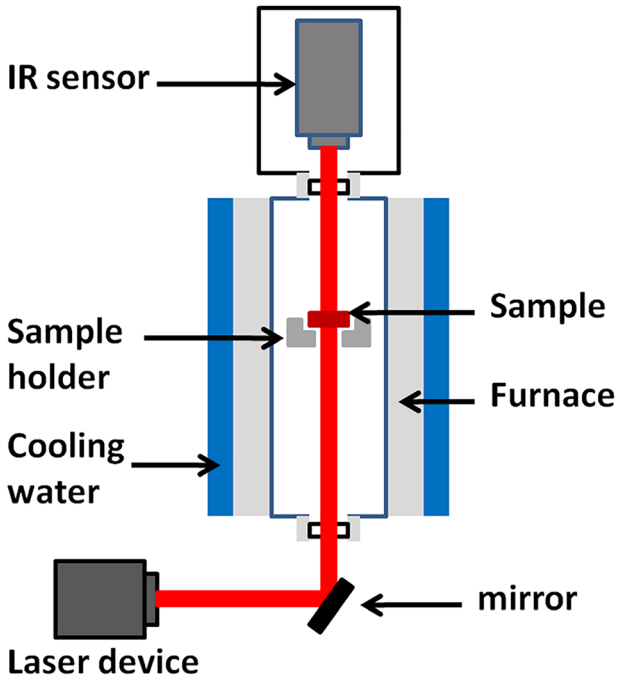

Fig. 1 A typical configuration of a laser flash system

side is then recorded by an infrared sensor. The specific experimental setup is based on the one-dimensional heat transfer assumption. One of the advantages of the laser flash method is that the diffusivity value may be calculated simply by one variable from testing and one sample dimension [16], as shown in Fig. 2

$$\alpha = 0.1388 \cdot L^2/t_{1/2} \tag{1}$$

where L is the thickness of the sample and $t_{1/2}$ is the time to reach the half of the maximum temperature. It should be mentioned that Eq. (1) gives just a simplified thermal diffusivity calculation using the Parker model [16] and there are more comprehensive models that account for minor heat loss using an analytical method for the diffusivity determination from the experimental data. Parker and other models do not depend on absolute temperature; therefore, the thermograms are normalized by dividing by the peak infrared sensor signal value for direct comparison of tests at varying setpoint temperatures.

Utilizing a laser flash system, Stryczniewicz et al. [17] estimated the thermal property of a coating material. The obtained experimental results were used as a basis in a multivariables identification procedure. Both an inverse heat transfer method and a numerical simulation were applied to determine the thermal diffusivity of the coating material in a coating-substrate-coating sample. Wright et al. [18] also conducted laser flash testing to evaluate the thermal diffusivity of a two-layered sample, which has the thermal diffusivity of one material unknown. The authors attempted to estimate the unknowns such as the thermal diffusivity and the input power by minimizing the difference between the numerical simulation and the measured data with a least-squared approach.

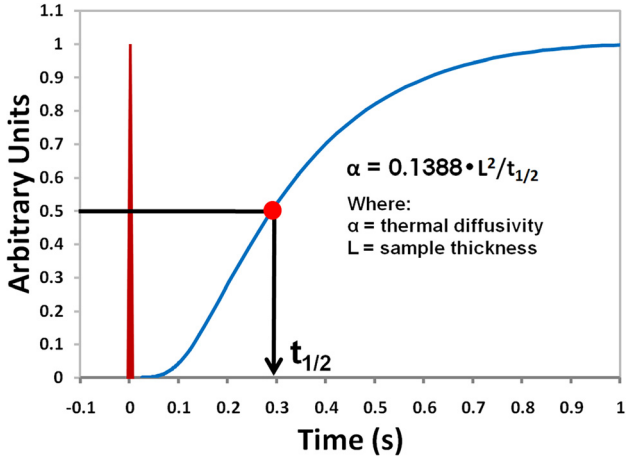

Fig. 2 Illustration of normalized output curve from thermal signals

Although there is a pool of literature focused on LPBF or EBAM build material properties, most of the reports are about the build part characteristics, such as the yield strength, hardness, and microstructures. The thermal properties, especially for powder materials, are less frequently found in literature. To estimate the powder conductivity in the EBAM process, Cheng et al. [1] fabricated both solid and powder-encapsulated samples by an Arcam S-12[1] system using Ti-6Al-4V powder. The thermal conductivity of both samples was then individually measured using a commercial model TPS 2500 S hot-disk analyzer. The powder conductivity of the powder-encapsulated sample was then obtained by the concept of "thermal resistance in series" with the known solid sample conductivity and the sample geometry. Comparing to the hot-disk measurement technique, on the other hand, the laser flash method has advantages of higher testing temperatures, noncontact measurements, shorter response time, and not requiring true temperature measurements, etc.

The purpose of this study is to develop a methodology combining both experimental and numerical approaches to evaluate the thermal diffusivity of metal powder used in LPBF as in powder bed conditions. The intent is to inversely obtain the powder thermal conductivity in LPBF through iterative heat transfer simulations of the laser-flash thermal response that matches closely to the data from the experiment.

Laser Flash Method

For the experimental approach, laser flash testing was employed to measure the thermal diffusivity of designed and fabricated specimens. Once the thermal diffusivity α is obtained, the thermal conductivity k is calculated from Eq. (2), related to the density ρ and the specific heat c_p

$$\alpha = \frac{k}{\rho \times c_p} \tag{2}$$

Laser flash testing was first conducted to a reference material to examine the combined experimental-numerical approach. Solid molybdenum (Mo) specimens were measured from room temperature up to 1600 °C. The disk-shaped specimens have a diameter and a thickness of 12.5 mm and 3.176 mm. A DLF-1600 laser flash system from TA Instruments,[2] shown in Fig. 3, was utilized to perform thermal diffusivity measurements. During testing, a laser pulse of 35 J is applied uniformly on the sample's top surface and lasts 0.001 s. Before the laser pulse, the furnace reaches a uniform temperature (within several degrees Celsius of the user-specified setpoint) for a certain duration to guarantee the entire sample itself has a constant initial temperature. On the other side of the sample, an infrared pyrometer collects thermal signals from the transient response.

The transient thermal data collected from the sample's bottom surface (nonheating side) was averaged and normalized. Figure 4 shows an example of both the raw data and the normalized curve from a testing temperature of 94.5 °C. A rapid temperature rise is

[2]Certain commercial entities, equipment, or materials may be identified in this document in order to describe an experimental procedure or concept adequately. Such identification is not intended to imply recommendation or endorsement by the National Institute of Standards and Technology, nor is it intended to imply that the entities, materials, or equipment are necessarily the best available for the purpose.

Fig. 3 DLF-1600 laser flash system

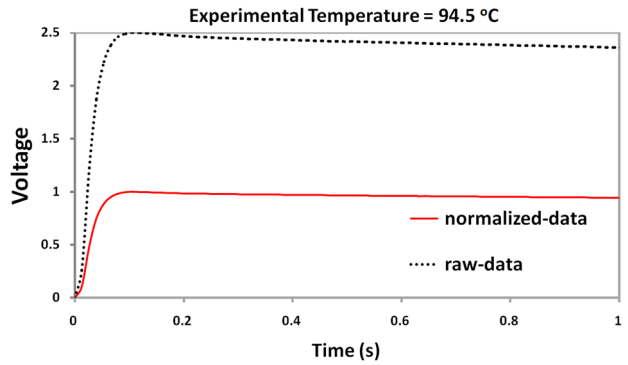

Fig. 4 Example of raw and normalized data curves from single-shot laser

noted, while temperature decrease after the laser shot is fairly slow, indicating relatively little heat loss of the measuring sample inside the furnace.

Finite Element Heat Transfer

A finite element (FE) method was applied to model the transient heat transfer of the laser flash process, using ABAQUS software to realize thermal simulations. The tested Mo sample was modeled according to its actual dimensions. One side of the sample was subject to a heat source from a laser pulse, which was simplified as a uniformly distributed surface heat flux. The laser irradiation area was approximated as a 10 mm diameter circle, estimated from the experiment. The furnace was filled with N_2 gas during testing, and thus, heat convection and thermal radiation were considered as the thermal boundary conditions. Moreover, the initial condition was assumed to be the actual testing temperature, uniform in the whole model. The environmental temperature was set to be the same as the testing temperature. The mesh size is about 0.166 mm by 0.166 mm by 0.166 mm in the laser irradiation region, as shown in Fig. 5. Temperature-dependent conductivity, specific heat, and density of the testing material, from literature and shown in Fig. 6,[3] were incorporated in the FE model. The material emissivity is 0.05 to 0.18 (unitless).[4] The convection coefficient is estimated to be 10 W/m^2 K [6]. The simulation result, the temperature field and history, was processed to obtain the average temperature at the surface that corresponds to the signal acquisition area on the sample, also about 10 mm diameter circle at the bottom surface.

[3]http://www-ferp.ucsd.edu/LIB/PROPS/PANOS/moa.html
[4]http://www.engineeringtoolbox.com/emissivity-coefficients-d_447.html

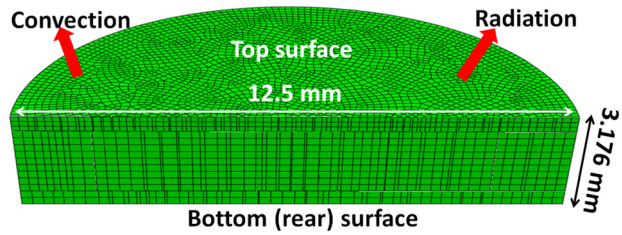

Fig. 5 Model mesh and boundary conditions

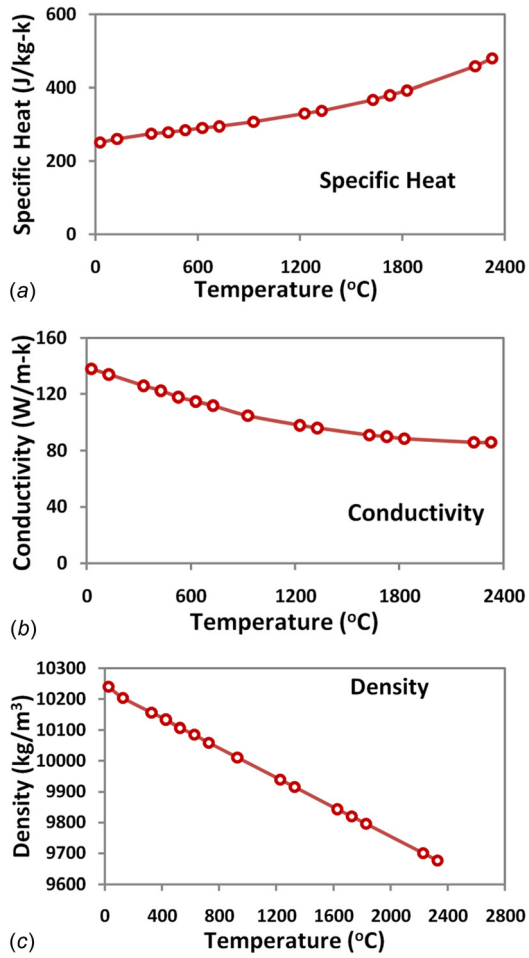

Fig. 6 Solid molybdenum material properties[3]

Simulations were conducted using the actual testing temperatures from the experiment to validate the FE model. The simulation and experimental results were compared, shown in Fig. 7, at both low and high temperatures. It can be observed that the normalized temperature response (T/T_{max}) curve from the simulation matches well to that from the experiment. There is a slight difference between the experiment and simulation only in the temperature decreasing stage. The minor deviation, which is more noticeable at a higher testing temperature, may be attributed to the simplified boundary condition of the sample, e.g., no heat dissipation from the sample holder contact. Nonetheless, the model is accurate in capturing the specimen diffusivity since $t_{1/2}$ is only related to the heating range. Diffusivity values measured by laser flash, direct output from the DLF-1600 system calculated using the Clark and Taylor model [19], at different temperatures were compared with literature data, summarized in Fig. 8, showing reasonable agreement between the two.

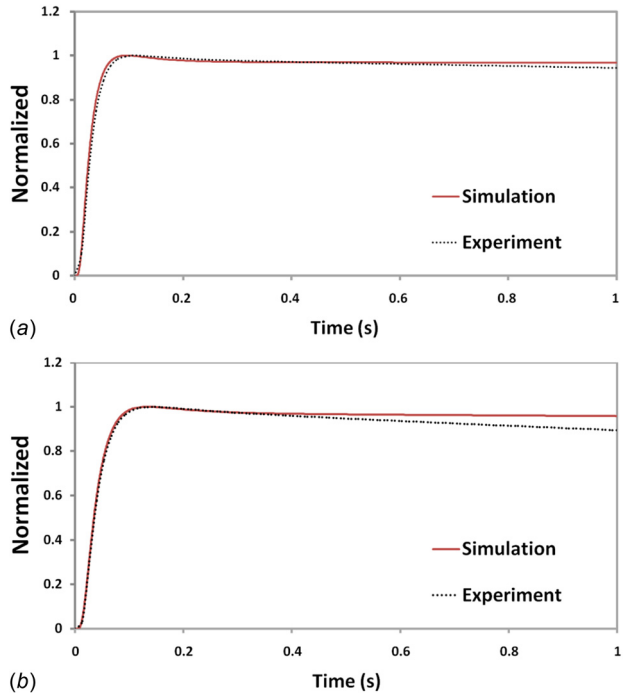

Fig. 7 Simulation versus experimental results at different testing temperatures (*a*) 94.5 °C, (*b*) 798.6 °C

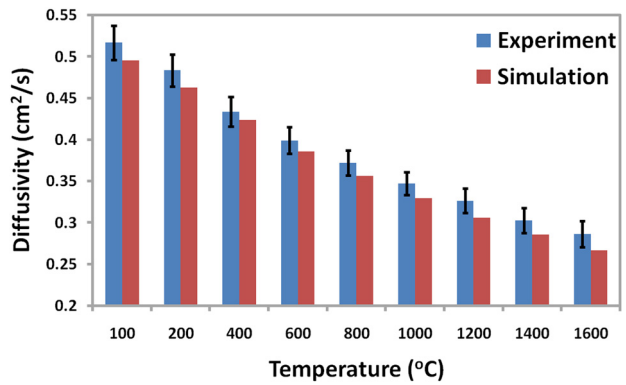

Fig. 8 Comparisons of measured thermal diffusivity with literature data [20] used in simulations. Error bars are standard uncertainty from Mo calibration material certificate.

Study of Powder Enclosed Samples

To study the LPBF powder thermal properties, a hollow disk model, 6.25 mm radius and 2 mm height with 0.25 mm and 0.5 mm shell thickness for the flat and circumferential surfaces, respectively, was created in computer-aided design (CAD) software. The geometric information of the model is shown in Fig. 9. The designed model was then fabricated using an LPBF system, EOS M270, with 17-4 stainless steel powder and default process parameters. The fabricated disk specimens contained the powder to be analyzed for thermal diffusivity. Laser flash testing was performed on the powder-enclosed specimens using the DLF-1600 to obtain the normalized thermal response curve. The result was then compared to the simulations with an attempt to determine the powder conductivity by matching the simulation with the experimental thermal response.

The developed FE thermal model was also modified based on the sample geometry and used to simulate laser flash testing of the powder-enclosed sample. Temperature-dependent thermal properties of solid 17-4 stainless steel were obtained from literature,

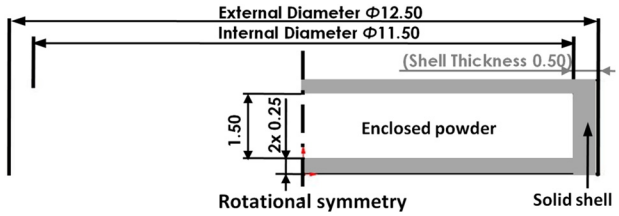

Fig. 9 Dimensional information (in mm) of the model for fabrication of powder-enclosed samples

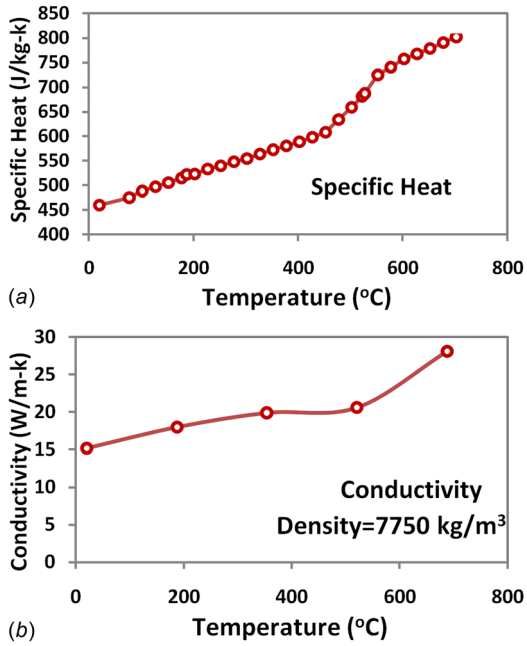

Fig. 10 Physical properties of solid 17-4 stainless steel [21,22]

Fig. 10, and included in the model. The 17-4 stainless steel emissivity was estimated as 0.3 [21]. The powder thermal conductivity value was to be determined and adjusted in the simulation so that to approach the simulated thermal response to the experimental curve.

One of the issues noted that may affect the simulation accuracy was the contact between the enclosed powder and the solid top shell. After LPBF fabrications, it is possible that sample handling may cause powder to settle due to gravity, resulting in a gap filled with nitrogen gas used in LPBF, and thus, poor contact between the powder region and the top shell, effectively thermally insulating the interface. In a similar study also using the laser flash technique for metallic powder thermal property analysis, Whiting et al. showed the existence of such a gap in powder-enclosed LPBF samples by computed tomography (CT) scanning [23]. To simulate the insulation condition, the contact conductance of extreme low value, e.g., 10^{-4} W/m^2 K, was tested to simulate the insulation due to the gas gap. The results from the experiment and simulation are compared in Fig. 11. It is found that the result is closely matched in the temperature rising range, indicating that the obtained $t_{1/2}$ time is similar to the laser flash measurements. However, the effective diffusivity obtained from this experiment may not be truly contributed by the powder diffusivity, since the insulated contact between the powder and the top shell would direct the heat flow toward and through the solid circumferential shell instead of the powder inside. Therefore, such a sample model is not suitable in analyzing the powder thermal conductivity and a different configuration of the model geometry that can improve the contact condition is needed.

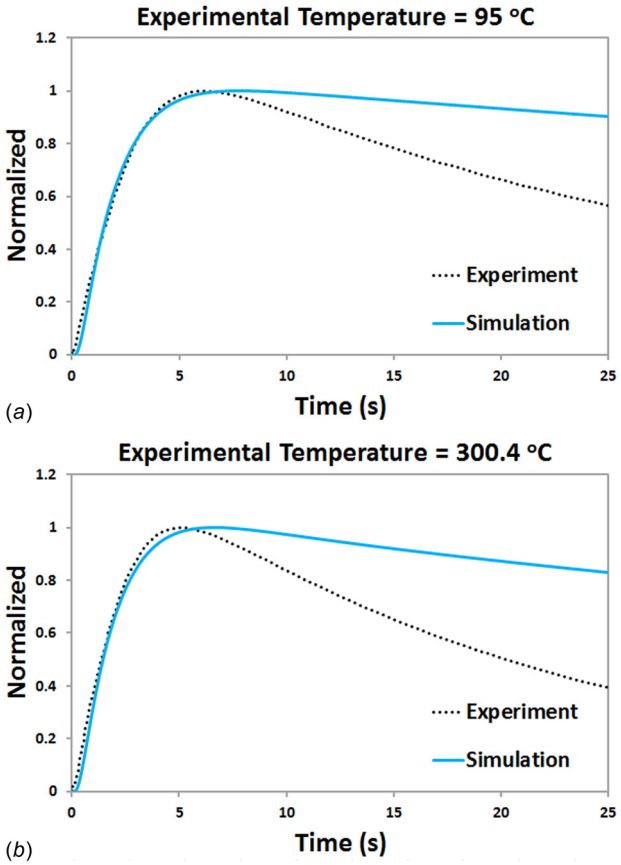

Fig. 11 Normalized thermal response curves from simulation and experiment for flat-surfaced powder-enclosed samples: (*a*) 95 °C and (*b*) 300.4 °C

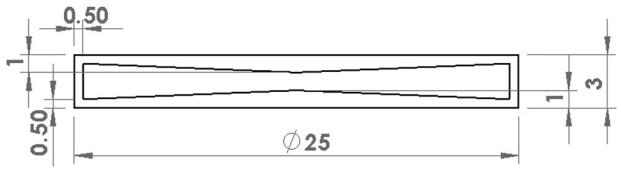

Fig. 12 Cross-sectional view of new sample design showing internal cones (unit: mm)

Sample Geometry Modification. To mitigate the possible gap-insulation issue, a new sample design was proposed. Figure 12 shows the cross-sectional view of the newly designed model; overall, it has a diameter of 25 mm and is 3 mm thick. The shell thickness is 0.5 mm all around (top/bottom/circumference). In addition, internal solid cones extended from both the top and bottom shells with a height of 0.5 mm were added. The intent is to reduce or minimize the gas gap between the powder section and the top shell. Further, the shape of the cones may help direct the heat flow toward the internal powder section.

The samples of the newly designed model were fabricated by an EOS M270 system using nickel alloy 625 powder. Laser flash testing was then performed to the samples using a DLF-1200 system from TA instruments (Fig. 13(*a*)). The system generates laser irradiation to the bottom surface of the sample with an input power of 25 J and a duration of 0.003 s, and has a pyrometer collecting the infrared signal from the opposite side (i.e., top surface). Both the powder-enclosed samples (with the cone feature) and solid samples (same overall dimensions as powder-enclosed samples) were tested at 500 °C. Figure 13(*b*) shows the normalized thermal responses from both the solid and powder-enclosed samples. The plots include the average of three consecutive tests

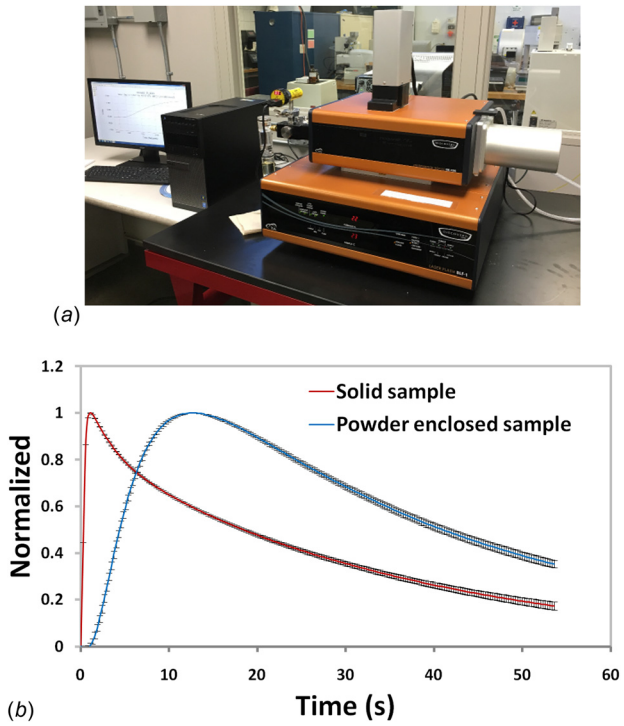

Fig. 13 (*a*) DLF-1200 laser flash apparatus and (*b*) normalized curves from testing of both solid and powder-enclosed samples

with standard deviation values, showing good repeatability, less than 5% in the temperature decreasing range for the powder-enclosed sample. The measured thermal diffusivity of the solid and powder-enclosed samples is 0.045 cm^2/s and 0.0028 cm^2/s, respectively, using the Clark and Taylor model [19].

The developed FE heat transfer model was modified accordingly to simulate the new samples and testing conditions. The sample material was updated with solid nickel alloy 625 properties [24].[5] To better account for heat loss in the transient heat transfer during laser flash testing, the alumina sample holder that a specimen sits on during testing was included in the FE model. Figure 14 shows the sample holder and its geometric information.

The measured thermal diffusivity of the powder-enclosed samples has the combined contribution from both the solid material (shell) and the powder (internal). Thus, an inverse method was proposed to analyze the powder thermal properties from the experimental results. The approach uses measurement data such as the temperature history to estimate unknown variables such as the powder thermal properties (the objective of the study) or model variables such as heat transfer coefficients of the boundary conditions. Moreover, there are additional variables that are not known and need to be determined simultaneously as well, e.g., thermal contact conductance between the powder and the solid shell. In this study, an inverse method based upon a multivariable, multipoint optimization algorithm was developed and applied to minimize the difference between the simulation and experimental results; a set of temperature data (at different times) from the experimental curve serves as the points for comparisons between the simulation and experiment. Further, an iteration scheme, using the Levenberg–Marquardt method [25], was employed to reach the optimal estimate of the unknowns through convergence of the simulation to the experimental data.

Thus, the estimation of the powder thermal conductivity involves two parts: (1) a direct problem of transient heat transfer in the laser flash process, which is solved by an FE simulation, and (2) an inverse problem of multiple unknowns, which will be

[5] http://www.hightempmetals.com/techdata/hitempInconel625data.php

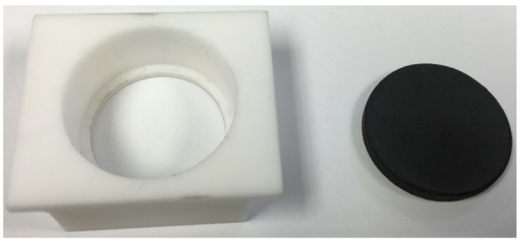

(*a*)

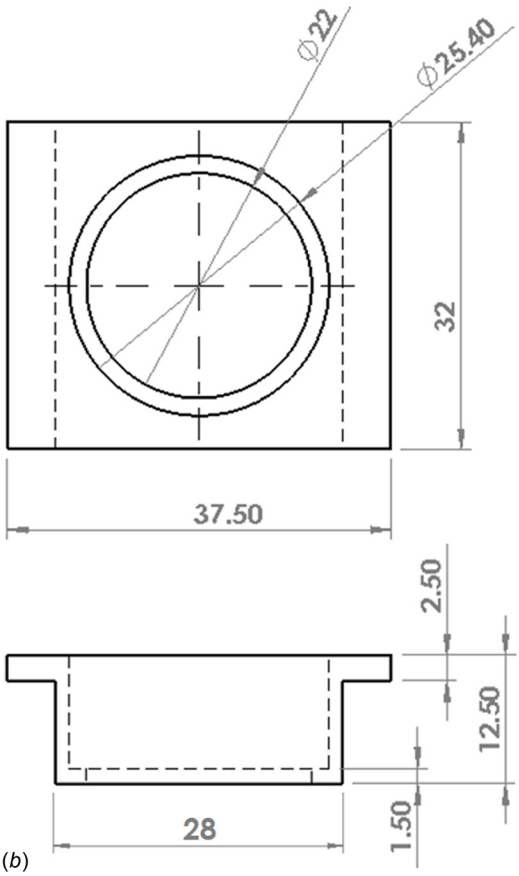

(*b*)

Fig. 14 (*a*) Sample holder and sample for testing and (*b*) dimensional information of sample holder (mm)

solved by, iteratively, a multipoint optimization algorithm. In part (1), the numerical simulation is obtained by incorporating variables from the previous iterative procedure. In part (2), the attempt of the inverse problem is to minimize the least squares equation [25]

$$S = \sum_{i=1}^{N} (T_{\exp-i} - T_{\text{sim}-i})^2 \tag{3}$$

where $T_{\text{sim}} = T(P_1, P_2, P_3, P_4, \ldots, P_m)$, P's are the unknown variables. $T_{\exp-i}$ means the measured output at a time-step (different specific points on the output curve), N is the total number of experimental data points for comparisons, and m is the total number of unknowns.

For the unknown estimation, the Levenberg–Marquardt iterative procedure was used; the equation for a new set of unknowns is given as follows

$$P^{n+1} = P^n + \left[(\mathbf{J}^n)^{\text{Tr}}\mathbf{J}^n + \mu^n\Omega^n\right]^{-1}(\mathbf{J}^n)^{\text{Tr}}[T_{\text{meas}} - T_{\text{est}}(P^n)]$$
$$\Omega^n = \text{diag}[(\mathbf{J}^n)^{\text{Tr}}\mathbf{J}^n] \tag{4}$$

where n is the current iteration number, μ^n is a user specified damping factor at current iteration, J is the matrix of sensitivity coefficients shown below (Eq. 5), and Ω^n is the diagonal matrix of the product of $\mathbf{J}^{\text{Tr}}$ (transpose of J) and J itself.

The coefficient J is defined as the first derivative of the estimated output at a specific time t, with respect to each unknown P in the current iteration

$$J = \begin{bmatrix} \frac{\partial T_{\text{est}-1}}{\partial P_1} & \frac{\partial T_{\text{est}-1}}{\partial P_2} & \cdots & \frac{\partial T_{\text{est}-1}}{\partial P_m} \\ \frac{\partial T_{\text{est}-2}}{\partial P_1} & \frac{\partial T_{\text{est}-2}}{\partial P_2} & \cdots & \frac{\partial T_{\text{est}-2}}{\partial P_m} \\ \vdots & \vdots & \vdots & \vdots \\ \frac{\partial T_{\text{est}-N}}{\partial P_1} & \frac{\partial T_{\text{est}-N}}{\partial P_2} & \cdots & \frac{\partial T_{\text{est}-N}}{\partial P_m} \end{bmatrix} \tag{5}$$

The first derivative values can also be computed using finite difference for a nonlinear condition, and thus, the sensitivity matrix can be calculated with the parameter increment of 1%

$$J_{ij} \cong \frac{T_{\text{est}-i}(P_1, P_2, \ldots, P_j + \Delta P_j, \ldots, P_m) - T_{\text{est}-i}(P_1, P_2, \ldots, P_j, \ldots, P_m)}{\Delta P_j} \tag{6}$$

The use of $\mu^n\Omega^n$ is to damp oscillations and instabilities during the calculation process by making a comparatively larger quantity to the result of $(\mathbf{J}^n)^{\text{Tr}}\mathbf{J}^n$. The damping factors may be made large during the beginning of iterative steps, since the initial guess of the unknowns can be quite different from the exact values. As the iterative procedure continues toward the optimal or true solutions, the damping factor may be reduced.

The inverse method aims at reducing the difference between the simulation and experimental results. An optimal solution can be considered, when the error S is the smallest. The iterative procedure is described in the following, with the process flow also shown in Fig. 15:

(1) Solve the direct problem by the FE model with the parameters $\mathbf{P}^n$ obtained from the previous iteration (or guess values for the initial iteration) to calculate the normalized temperature response versus time;
(2) Calculate $S(\mathbf{P}^n)$ value;

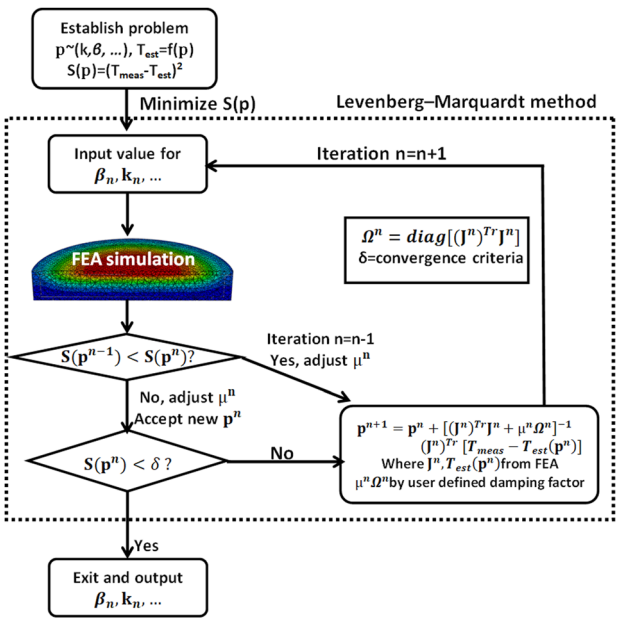

Fig. 15 Optimization process flow for unknown estimation

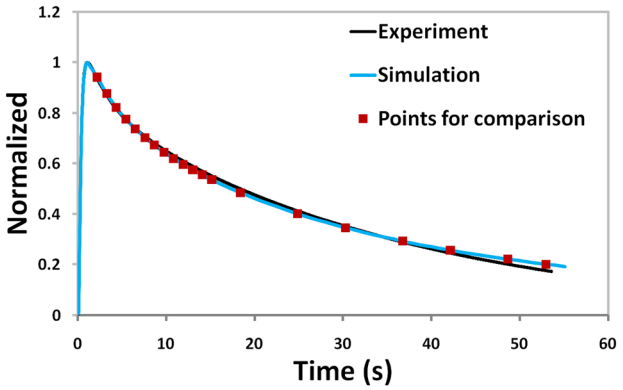

Fig. 16 Normalized temperature versus time for solid sample analysis to obtain the contact conductance between the sample and the sample holder

(3) Compute the sensitivity matrix **J** by using the current value of $\mathbf{P}^n$;
(4) Solve for the newly estimated $\mathbf{P}^{n+1}$;
(5) Solve the FE model again by using new $\mathbf{P}^{n+1}$ values and calculate $S(\mathbf{P}^{n+1})$;
(6) If $S(\mathbf{P}^{n+1}) > S(\mathbf{P}^n)$, adjust the damping factor to attain another set of $\mathbf{P}^{n+1}$(then go to step 4), and if not, accept $\mathbf{P}^{n+1}$ values for the next iteration;
(7) If $S(\mathbf{P}^{n+1})$ is smaller than the user specified error allowance or cannot be further reduced, then stop the iteration process and output the final $\mathbf{P}^{n+1}$ values (i.e., optimal solution); if not, repeat step (1) to (6).

To begin with the inverse method, unknown variables need to first be identified so that to be included in the iteration process. In the current study, initially, five unknown variables were identified: powder thermal conductivity (k), powder bed density (ρ), and contact conductance values: (i) between the top cone and internal powder (k_t), (ii) between the bottom cone and internal powder (k_b), as well as (iii) between the testing sample and the sample holder (k_s). The variable k_s can be obtained from the analysis of solid sample testing and the corresponding heat transfer simulation, in which the only unknown is k_s. Therefore, the study, both testing and simulations, was first conducted to the solid nickel alloy 625 sample made by the same LPBF system. To quantify the difference between a simulation and an experimental set, 20 points in the normalized thermal history curve, at specified time intervals, were used to calculate the squared error value (S) between the simulation and experiment, calculated from Eq. (3). It was found that k_s at 4500 W/m^2 K reaches the minimum S value at the testing temperature of 500 °C, with the final result shown in Fig. 16. The calculated k_s value will then be used for the study of the powder-enclosed samples.

With the sample and holder contact conductance obtained, there are four unknowns to be determined for the analysis of the powder-enclosed sample, i.e., k, ρ, k_t and k_b. Same as the solid sample analysis, 20 points from the experimental results (corresponding times shown in Fig. 17(*b*), roughly 10 points in both of temperature increasing and decreasing durations) were used in the multipoint optimization method for the comparison purpose. During each iteration, a damping factor is adjusted to obtain the four variables for the next iteration. The new variables will be input into the FE model to perform simulations and obtain new output. The S value will be calculated so as to make sure that it is smaller than the previous iteration. If the current S value is greater than the one from the previous iteration, the four variables need to be recalculated again from the previous iteration. When the S value is smaller than an allowed error (stopping criterion) or cannot be further reduced, the iteration will stop. Figure 17 shows the evolution of the simulated thermal response curve along the iteration steps, and Table 1 is the summary of the results of the variables

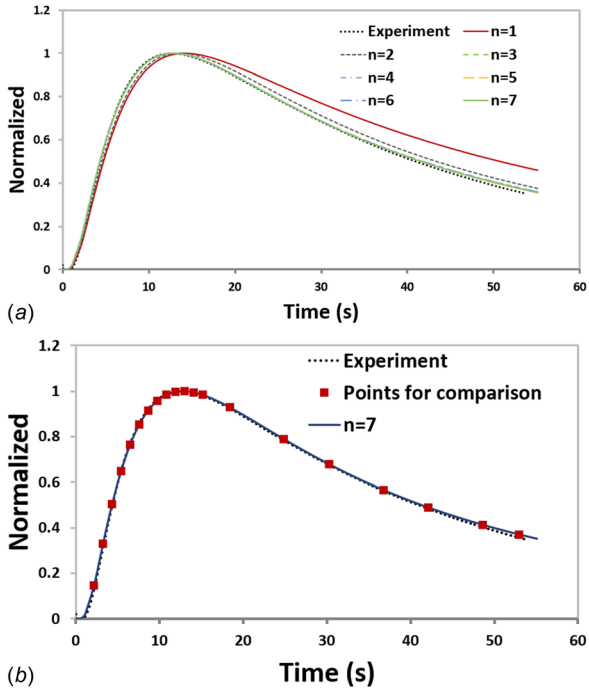

Fig. 17 Result from powder-enclosed sample analysis (500 °C): (*a*) comparison between different iterations and (*b*) final simulation result comparison with experiment

and error from each iteration; the values for the initial iteration were some guessing values.

It can be noted, from Table 1, that the solution of unknowns tends to converge in just a few iterations. At the seventh iteration, the least squared error (S) has reached a small value ($S < 0.002$, which is roughly equivalent to less than 1% difference, in average, of 20 points of normalized temperatures). Thus, it is considered that the result obtained from $n = 7$ is the optimal solution. Future work will implement a more quantitative means for the converging criterion of optimal solutions. From the study thus far, the thermal conductivity of nickel alloy 625 powder at 500 °C can be estimated as 1.01 W/m K. The calculated powder thermal conductivity is substantially lower than that of solid nickel alloy 625 at 500 °C (19.6 W/m K), only about 5%. The solid-powder contact conductance values are estimated to be 634 W/m^2 K and 801 W/m^2 K for the top and bottom shells, respectively. In addition, the powder bed density is estimated as 4459 kg/m^3, equivalent to a porosity of 46%. The proposed method, which aims at fitting the numerical simulation with the experimental response curve, provides a practical method to analyze the thermal properties of powder materials, based on a transient heat transfer process. It extends the measurement capability of the laser flash method to compacted metallic powder without a specially designed powder holder. The feasibility of this method has been demonstrated by analyzing the powder thermal conductivity

Table 1 Values of unknowns and errors from different iterations

Iteration No.	k W/m K	k_t W/m^2 K	k_b W/m^2 K	ρ kg/m^3	S
	0.1	100	100	826	0.322
1	1.12	1480	514	7751	0.0839
2	0.944	576	726	4707	0.0137
3	1.10	650	809	4711	0.00258
4	1.08	643	803	4661	0.00238
5	1.06	640	802	4611	0.00224
6	1.04	637	801	4525	0.00202
7	1.01	634	801	4459	0.00188

through the iterative process. The significant difference in thermal conductivity between metal powder bed and its solid counterpart has been proved using the developed method.

Conclusions

Knowing the powder thermal conductivity in LPBF is essential for accurate thermal process modeling. However, it is a challenging task to measure the powder thermal conductivity as in powder bed conditions. In this study, an approach that combines laser flash testing, FE transient heat transfer modeling, and a multivariables inverse method was developed and applied to analyze the thermal conductivity of nickel alloy powder enclosed in samples fabricated by an LPBF system using default process parameters. The major findings are summarized as follows.

(1) Thermal diffusivity of a reference material (Mo) measured by laser flash testing is very close to the reference data across a wide range of temperatures.
(2) FE modeling of transient heat transfer in the laser flash process was validated by the experiment, matching well with the normalized thermal response from testing of the Mo sample.
(3) For powder-enclosed sample testing, the sample internal geometry was modified to minimize the gap that came from powder settling causing adiabatic-like contact, which affects the measurement results. The modified internal geometry includes internal cones, one at top and the other at bottom, of 0.5 mm height.
(4) As an example, the thermal conductivity of nickel alloy 625 from LPBF was analyzed to be 1.01 W/m K at 500 °C, only about 5% of the thermal conductivity for solid nickel alloy 625. In addition, the powder bed porosity is estimated to be 46%.
(5) The developed algorithm for the inverse method involving multiple unknowns is effective, seven iterations to reach less than 0.2% of a total squared error of 20 points from the thermal response curve.

To examine the robustness of the developed methodology for the powder thermal conductivity analysis, future work will be extended to (1) different temperatures, (2) various internal features in powder-enclosed samples, and (3) other powder materials, e.g., Ti-6Al-4V. Error analysis and propagation will be examined to investigate the measurement uncertainty.

Acknowledgment

The authors thanked Drs. Alkan Donmez and Shawn Moylan for very helpful discussions. Part of numerical work in this study was conducted using the resources in the University of Louisville's research computing group and the Cardinal Research Cluster.

Funding Data

- National Institute of Standards and Technology (70 NANB16H029).

References

[1] Cheng, B., Price, S., Lydon, J., Cooper, K., and Chou, K., 2014, "On Process Temperature in Powder Bed Electron Beam Additive Manufacturing: Model Development and Validation," ASME J. Manuf. Sci. Eng., **136**(6), p. 061018.
[2] Jamshidinia, M., Kong, F., and Kovacevic, R., 2013, "Numerical Modeling of Heat Distribution in the Electron Beam Melting® of Ti-6Al-4V," ASME J. Manuf. Sci. Eng., **135**(6), p. 061010.
[3] Fu, C., and Guo, Y., 2014, "Three-Dimensional Temperature Gradient Mechanism in Selective Laser Melting of Ti-6Al-4V," ASME J. Manuf. Sci. Eng., **136**(6), p. 061004.
[4] Yuan, P., and Gu, D., 2015, "Molten Pool Behaviour and Its Physical Mechanism During Selective Laser Melting of TiC/AlSi10 Mg Nanocomposites: Simulation and Experiments," J. Phys. D, **48**(3), p. 035303.
[5] Romano, J., Ladani, L., Razmi, J., and Sadowski, M., 2015, "Temperature Distribution and Melt Geometry in Laser and Electron-Beam Melting Processes–A Comparison Among Common Materials," Addit. Manuf., **8**, pp. 1–11.
[6] Cheng, B., Shrestha, S., and Chou, K., 2016, "Stress and Deformation Evaluations of Scanning Strategy Effect in Selective Laser Melting," Addit. Manuf., **12**, pp. 240–251.
[7] Cheng, B., and Chou, K., 2015, "Geometric Consideration of Support Structures in Part Overhang Fabrications by Electron Beam Additive Manufacturing," Comput.-Aided Des., **69**, pp. 102–111.
[8] Zäh, M. F., and Lutzmann, S., 2010, "Modelling and Simulation of Electron Beam Melting," Prod. Eng., **4**(1), pp. 15–23.
[9] Roberts, I. A., Wang, C. J., Esterlein, R., Stanford, M., and Mynors, D. J., 2009, "A Three-Dimensional Finite Element Analysis of the Temperature Field During Laser Melting of Metal Powders in Additive Layer Manufacturing," Int. J. Mach. Tools Manuf., **49**(12–13), pp. 916–923.
[10] Lin, T. H., Watson, J. S., and Fisher, P. W., 1985, "Thermal Conductivity of Iron-Titanium Powders," J. Chem. Eng. Data, **30**(4), pp. 369–372.
[11] Sih, S. S., and Barlow, J. W., 2004, "The Prediction of the Emissivity and Thermal Conductivity of Powder Beds," Part. Sci. Technol., **22**(3), pp. 291–304.
[12] Kolossov, S., Boillat, E., Glardon, R., Fischer, P., and Locher, M., 2004, "3D FE Simulation for Temperature Evolution in the Selective Laser Sintering Process," Int. J. Mach. Tools Manuf., **44**(2–3), pp. 117–123.
[13] Patil, R. B., and Yadava, V., 2007, "Finite Element Analysis of Temperature Distribution in Single Metallic Powder Layer During Metal Laser Sintering," Int. J. Mach. Tools Manuf., **47**(7–8), pp. 1069–1080.
[14] Tolochko, N. K., Arshinov, M. K., Gusarov, A. V., Titov, V. I., Laoui, T., and Froyen, L., 2003, "Mechanisms of Selective Laser Sintering and Heat Transfer in Ti Powder," Rapid Prototyping J., **9**(5), pp. 314–326.
[15] Hadley, G. R., 1986, "Thermal Conductivity of Packed Metal Powders," Int. J. Heat Mass Transfer, **29**(6), pp. 909–920.
[16] Parker, W., Jenkins, R., Butler, C., and Abbott, G., 1961, "Flash Method of Determining Thermal Diffusivity, Heat Capacity, and Thermal Conductivity," J. Appl. Phys., **32**(9), pp. 1679–1684.
[17] Stryczniewicz, W., Zmywaczyk, J., and Panas, A. J., 2017, "Inverse Problem Solution for a Laser Flash Studies of a Thin Layer Coatings," Int. J. Numer. Methods Heat Fluid Flow, **27**(3), pp. 698–710.
[18] Wright, L., Yang, X.-S., Matthews, C., Chapman, L., and Roberts, S., 2011, "Parameter Estimation From Laser Flash Experiment Data," *Computational Optimization and Applications in Engineering and Industry*, Springer, Berlin, Germany, pp. 205–220.
[19] Clark, III, L., and Taylor, R., 1975, "Radiation Loss in the Flash Method for Thermal Diffusivity," J. Appl. Phys., **46**(2), pp. 714–719.
[20] TA Instruments, 2017, "Thermal Diffusivity Calibration Date Sheet of NIST Traceable Molybdenum Reference," TA Instruments, New Castle, DE.
[21] Li, Y. Y., and Hwang, W. S., 2008, "Numerical Simulation of the Solidification Microstructure of a 17-4PH Stainless Steel Investment Casting and Its Experimental Verification," Modell. Simul. Mater. Sci. Eng., **16**(4), p. 045009.
[22] Rack, H., 1981, "Physical and Mechanical Properties of Cast 17-4 PH Stainless Steel," Sandia National Labs, Albuquerque, NM, Report No. SAND-80-2302, TTC-0161.
[23] Whiting, J., Lane, B., Chou, K., and Cheng, B., 2017, "Thermal Property Measurement Methods and Analysis for Additive Manufacturing Solids and Powders," SFF Symposium, Austin, TX, Aug. 7–9, pp. 29–38.
[24] Capriccioli, A., and Frosi, P., 2009, "Multipurpose ANSYS FE Procedure for Welding Processes Simulation," Fusion Eng. Des., **84**(2–6), pp. 546–553.
[25] Ozisik, M. N., and Orlande, H. R. B., 2000, *Inverse Heat Transfer*, Taylor and Francis, New York.